24th INTERNATIONAL CONGRESS ON SOUND AND VIBRATION
23–27 July 2017, London

ICSV24
23-27JULY 2017
LONDON CALLING

ADAPTIVE CONTROL OF RADIATED SOUND POWER BASED ON TIME-DOMAIN ESTIMATES OF ACOUSTIC RADIATION MODES

Khairul A. M. Nor

University of Auckland, Department of Mechanical Engineering, Auckland 1142, New Zealand

International Islamic University Malaysia, 53100 Kuala Lumpur, Malaysia

email: kmdn813@aucklanduni.ac.nz

Brian R. Mace

University of Auckland, Department of Mechanical Engineering, Auckland 1142, New Zealand

Yusuke Hioka

University of Auckland, Department of Mechanical Engineering, Auckland 1142, New Zealand

In active structural acoustic control, broadband control of the radiated sound power from a structure can be achieved by minimizing the amplitudes of the acoustic radiation modes (ARMs). The shape of these ARMs is frequency dependent and only a few might radiate significant power in a given frequency range. In this paper a method is described by which the ARMs are estimated in real-time from a number of point response measurements taken on a vibrating structure. These estimates can be used to calculate the radiated power or, here, in a feedforward adaptive control system. Estimates of the ARM amplitudes in the time domain are produced by digitally filtering the outputs of an array of sensors mounted on the radiator. These filters are designed by FIR filters in the frequency domain based on the frequency-dependent ARMs and implemented in the time domain. These estimates are then used as the cost function in a feedforward, adaptive, filtered-X LMS controller. The theory is described with reference to a 2-dimensional vibrating structure. Finally numerical results of real-time simulations are presented.
Keywords: Acoustic radiation modes, real-time control, FxLMS controller.

1. Introduction

In real-time applications of active structural acoustic control (ASAC), the accuracy of estimating the radiated sound power of the vibrating structure is vital. The sound power generated by a vibrating structure can be measured as a superposition of its velocity distributions that radiate power independently to the acoustic far-field [1-2]. These velocity distributions are called acoustic radiation modes (ARMs). Physically, they are basis vectors orthogonal to each other in vector space, and each basis vector represents a particular velocity pattern. They are functions of position and frequency only but not boundary conditions, hence are not dependent on the natural modes of the radiating structure. Theoretically, due to their orthogonality, reducing the radiated sound power from the ARMs with higher radiation efficiencies can give a significant overall attenuation of the sound power.

The majority of previous work concerns discrete frequency or frequency-domain methods. However, a problem occurs when the frequency dependent features of ARMs and their radiation efficiencies are considered in broadband, real-time control applications. Unlike frequency-domain approaches, estimating ARMs in the time-domain enables a broader frequency range of approximation

and thus reduces the controller dimensionality in ASAC system [3]. References [3-5] were among the few studies concerning estimating ARMs and the radiated sound power in the time-domain. Recently, Nor *et al.* [6] used time-domain estimates of the ARMs to approximate the radiated sound power of a baffled beam in a real-time simulation. The study managed to attenuate the radiated sound power from the first three ARMs using a feedforward control scheme.

This research extends the work of [6] and focuses on developing adaptive filtered-x least mean square (FxLMS) controllers to reduce the radiated sound power of a 2-D vibrating structure, e.g. a baffled clamped plate. The objective of this adaptive control is to minimise the instantaneous mean square ARM amplitudes, often the first few orders, hence cancelling the radiated sound power contributed by these ARMs. The theoretical background is described in Section 2. The method of estimating ARMs in the time-domain is presented in Section 3. Section 4 discusses the development of an adaptive controller using the FxLMS algorithm. Then, results of real-time simulations are presented in Section 5. Finally, Section 6 concludes this paper.

2. Theory

2.1 Acoustic radiation modes and radiated sound power

Consider a vibrating structure radiating sound into a surrounding acoustic field. If the surface of the structure is discretised into *N* elements, each considered to radiate in a piston-like manner, the radiated acoustic power is given by [1-2]

$$W = \mathbf{y}^H \mathbf{\Lambda} \mathbf{y} = \sum_{r=1}^{R} |y_r|^2 \lambda_r , \tag{1}$$

where $\mathbf{y} = \{y_1 \dots \dots y_R\}^T = \mathbf{Q}^T \mathbf{v}$ is the vector of ARM amplitudes, $\mathbf{Q}$ is the *N* x *R* matrix of ARMs, *N* and *R* are the total number of radiating elements and ARMs, respectively, $\mathbf{v}$ is the velocity vector and $\mathbf{\Lambda} = \{\lambda_1 \dots \dots \lambda_r\}^T$ is the vector of the eigenvalues of the radiation resistance matrix. The ARM amplitudes are functions of position and frequency only but not boundary conditions, hence are not dependent on the natural modes of the radiating structure. A detailed mathematical derivation can be found in [1].

Assuming the radiator is discretised into *N* elements of equal area, the radiation efficiency of the individual ARM is given by [7]

$$\sigma_r = 2N\lambda_r / (\rho_0 c_0 A), \tag{2}$$

where ρ_0 is the air density, c_0 is the sound velocity in the fluid, and *A* is the total surface area of the radiator.

2.2 Radiating structure

In this paper, a rectangular plate clamped at all edges is selected as the radiating structure. The plate lies in the region $0 \le x \le L_x$ and $0 \le y \le L_y$ and is subjected to a primary harmonic point force of amplitude F_p applied at (x_0, y_0). The surface velocity at the n^{th} location (x_n, y_n) is [7]

$$V_n(x, y, \omega) = F_p \sum_{q=1}^{\infty} \sum_{p=1}^{\infty} i\omega \left(\omega_{pq}^2 (1 + i\eta_{pq}) - \omega^2\right)^{-1} \varphi_{pq}(x_0, y_0) \varphi_{pq}(x_n, y_n), \tag{3}$$

where ω is the angular frequency, p and q are the mode number in *x*- and *y*-directions, respectively, and η_{pq} is the plate's modal loss factor. The mode shapes $\varphi_{pq}(x, y)$ can be well approximated by the product of two independent beam functions $\varphi_{pq}(x, y) = \phi_p(x)\phi_q(y)$. For a clamped plate, $\phi_p(y)$ and $\phi_q(x)$ are defined as [8]

$$\phi_p(x) = \cosh(\alpha_p x / L_x) - \cos(\alpha_p x / L_x) - \beta_p \left[\sinh(\alpha_p x / L_x) - \sin(\alpha_p x / L_x)\right],$$

$$\phi_q(y) = \cosh(\alpha_q y/L_y) - \cos(\alpha_q y/L_y) - \beta_q\left[\sinh(\alpha_q y/L_y) - \sin(\alpha_q y/L_y)\right], \tag{4}$$

while the $(p, q)^{\text{th}}$ natural frequency ω_{pq} of the plate is given by

$$\omega_{pq} = \sqrt{D/m_s}\cdot\sqrt{(I_1 I_2 + 2I_3 I_4 + I_5 I_6)/(I_2 I_6)}\,, \tag{5}$$

where m_s and D are the mass per unit area and bending stiffness of the plate, respectively, and

$$I_1 = \int_0^{L_x} \phi_p''''(x)\phi_p(x)dx\,, \quad I_2 = \int_0^{L_y} \left(\phi_q(y)\right)^2 dy\,, \quad I_3 = \int_0^{L_x} \phi_p''(x)\phi_p(x)dx\,,$$

$$I_4 = \int_0^{L_y} \phi_q''(y)\phi_q(y)dy\,, \quad I_5 = \int_0^{L_y} \phi_q''''(y)\phi_q(y)dy\,, \quad I_6 = \int_0^{L_x} \left(\phi_p(x)\right)^2 dx\,. \tag{6}$$

2.3 Numerical examples

Figure 1 shows the first two ARM shapes of the rectangular plate (L_y / L_x = 0.75) when the plate is excited at dimensionless frequency kl of 0.1, 1, 5 and 10 where l= L_x. In this figure, the first ARM is nearly uniform over the surface of the panel at low frequencies, i.e. $kl \leq$ l, whereas it is distorted towards a dome-shape at higher frequencies. The following modes are rocking-type dipole-like modes oriented along the two axes of the panel at low frequencies and become distorted as the frequency increases.

The radiation efficiency of the first five ARMs of the plate is shown in Fig. 2. From this figure, the lower ARMs are seen to be more efficient radiators at low frequencies; in other words, they contribute more to the radiated sound power than the higher ARMs. Thus, controlling those lower ARMs is most important to reduce the radiated sound power at low frequencies.

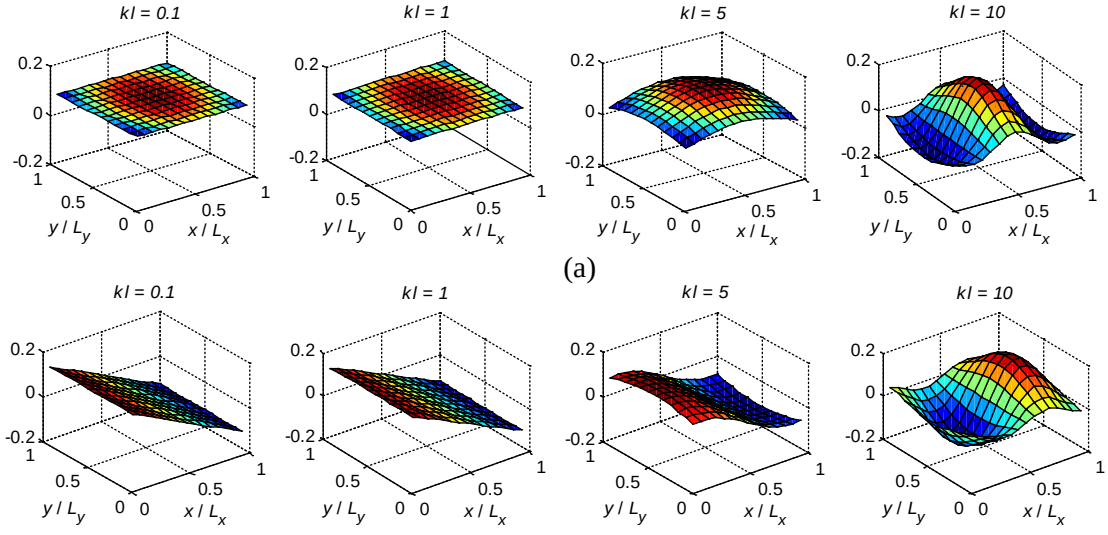

(a)

(b)

Figure 1: (a) First and (b) second ARMs of a rectangular plate structure when the dimensionless frequency is set to kl = 0.1, 1, 5 and 10, respectively.

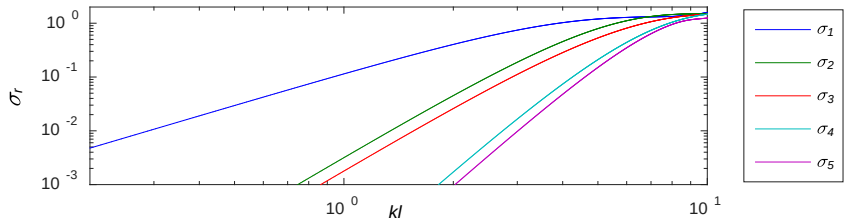

Figure 2: Radiation efficiencies of individual ARMs

3. Acoustic radiation mode filters

The ARMs are frequency-dependent, thus the ARM amplitude can be written in the frequency domain as

$$\mathbf{y}(\omega) = \mathbf{Q}(\omega)^T \mathbf{v}(\omega). \tag{7}$$

Suppose N_s structural sensors are used to estimate the radiation modes, hence Eq. (7) becomes

$$\begin{bmatrix} Y_1(\omega) \\ \vdots \\ Y_r(\omega) \\ \vdots \\ Y_R(\omega) \end{bmatrix} \approx \begin{bmatrix} Q_{1,1}(\omega) & \cdots & Q_{1,n}(\omega) & \cdots & Q_{1,N_s}(\omega) \\ \vdots & \ddots & & & \vdots \\ Q_{r,1}(\omega) & & \ddots & & Q_{r,N_s}(\omega) \\ \vdots & & & \ddots & \vdots \\ Q_{R,1}(\omega) & \cdots & Q_{R,n}(\omega) & \cdots & Q_{R,N_s}(\omega) \end{bmatrix} \begin{bmatrix} V_1(\omega) \\ \vdots \\ V_{n_s}(\omega) \\ \vdots \\ V_{N_s}(\omega) \end{bmatrix}, \tag{8}$$

where $V_n(\omega)$ is the velocity of the n^{th} sensor and $Q_{r,n}(\omega)$ is the value of the r^{th} ARM at the n^{th} sensor location. In real-time, the ARM amplitude, $y_r(t)$ is given by [6]

$$y_r(t) \approx \sum_{n=1}^{N_s} q_{r,n}(t) * v_n(t), \tag{9}$$

where $q_{r,n}(t)$ and $v_n(t)$ are the inverse Fourier transforms of $Q_{r,n}(\omega)$ and $V_n(\omega)$, respectively, and * denotes a convolution. This implies the ARM amplitude can be calculated by applying a filter whose impulse response is $q_{r,n}(t)$ to the sensor velocities. In digital applications, the ARMs can be estimated at discrete times $t=m\tau$ with a sampling frequency of $f_s=1/\tau$, hence Eq. (9) becomes

$$y_r(m) \approx \sum_{n=1}^{N_s} \left\{ \sum_{s=-\infty}^{+\infty} q_{r,n}(s) v_k(m-s) \right\}, \tag{10}$$

where $y_r(m)$ is the r^{th} ARM amplitude at time sample m and $q_{r,n}(s)$ is the value of $q_{r,n}(t)$ sampled at the sampling frequency f_s. Due to finite approximation using a FIR filter, the infinite sum is truncated. Given that $Q_{r,n}(\omega)$ always has zero phase, the best approximation will have $q_{r,n} = q_{r,-n,}$ but this implies the FIR filter will be non-causal. However, for real time implementation, the filter must be causal, i.e. $q_{r,n}(s) = 0$ for all $s < 0$, which leads to the approximated ARM amplitude estimate

$$y_r(m) \approx \sum_{n=1}^{N_s} \left\{ \sum_{s=0}^{S} q_{r,n}(s) v_k(m-s) \right\}. \tag{11}$$

The causal FIR filter in Eq. (11) will never be better than a non-causal filter that uses future values of v_k, i.e. for $s < 0$, because causality adds a constraint to the approximation. To make a non-causal yet practically realisable filter for real-time implementation, a causal version of the filter is introduced by delaying the non-causal filter by d samples [9]. This new filter will approximate a frequency response $Q_{r,n}(\omega)\exp(-i\omega d/f_s)$ and will produce an approximation of $y_r(m)$ at time sample $m+d$ and at the same time uses $(2d+1)$ coefficients for the optimal estimation of $Q_{r,n}(\omega)$ in the least square sense, i.e.

$$y_r(m) \approx \sum_{n=1}^{N_s} \left\{ \sum_{s=0}^{2d} q_{r,n}(s) v_k(m-s-d) \right\}. \tag{12}$$

For certain applications, such as in estimating the radiated sound power or using the ARM amplitude as an error function in adaptation schemes, allowing d samples delay to derive an ARM estimate will not be critical.

4. Adaptive feedforward active structural acoustic control

In this paper, adaptive, feedforward, active structural acoustic control is employed to reduce the sound power radiated by the vibrating rectangular plate. This is realized by j secondary control forces, F_s applied to the structure.

4.1 ARM amplitude as cost function

The lower order ARMs are more efficient in radiating sound and hence contribute more to the radiated sound power. Thus, reducing the first j ARM amplitudes using j control forces can give significant attenuation [7]. Ideally all first j ARM amplitudes should be zero, so that Eq. (7) gives

$$\mathbf{y}_c = \mathbf{Q}_c{}^T \mathbf{v} = \mathbf{0}, \tag{13}$$

where $\mathbf{Q}_c = \{\mathbf{Q}_1 \ldots \ldots \mathbf{Q}_j\}_c^T$ and $\mathbf{y}_c = \{y_1 \ldots \ldots y_j\}_c^T$ refer to the controlled ARMs and ARM amplitudes, respectively. Furthermore, the velocity can be divided into parts caused by the primary and secondary forces, $\mathbf{v}_p$ and $\mathbf{v}_s$, respectively, as

$$\mathbf{v} = \mathbf{v}_p + \sum_j \mathbf{v}_{s,j} = \mathbf{h}_p F_p + \mathbf{H}_s \mathbf{f}_s, \tag{14}$$

where $\mathbf{h}_p = \{H_1 \ldots \ldots H_N\}_p^T$ is the vector of sensor transfer functions due to the primary force F_p, $\mathbf{f}_s = \{F_1 \ldots \ldots F_j\}_s^T$ is the vector of the secondary forces, and $\mathbf{H}_s = \{\mathbf{h}_1 \ldots \ldots \mathbf{h}_N\}^T$ is the matrix of the sensor transfer functions due to the secondary forces. Substituting Eq. (14) into Eq. (13) and rearranging, the sound power radiated by the j^{th} ARM can be cancelled by reducing the j ARM amplitudes to zero, i.e.

$$\mathbf{y}_c = \left| \mathbf{Q}_c{}^T \mathbf{H}_p F_p + \mathbf{Q}_c{}^T \mathbf{H}_s \mathbf{F}_s \right| = \mathbf{0}, \tag{15}$$

The cost function will be defined in the form

$$J = \mathbf{y}_c{}^T \mathbf{y}_c. \tag{16}$$

4.2 Adaptive controller

The strategy to control the radiated sound power proposed here is realised by the application of feedforward adaptive control based on the filtered-X LMS algorithm. Here, two FIR filters are required. The first filter is the controller filter, used to cancel the ARM amplitude of the primary path, $G_{p,j}$, from the input signal $u(m)$ to the error signal $e(m)$. In this paper, the error signal is also the ARM amplitude $y(m)$. The second filter is the estimator of the secondary path $\hat{G}_{s,j}$, from the controller output to the error signal. This requires pre-filtering the reference signal in order to make the measured error signal and the filtered reference signal aligned in time to compensate for the dynamics of the secondary path.

The updated weights of the first FIR filter are calculated from [10]

$$\mathbf{w}(m+1) = \mathbf{w}(m) + 2 \cdot \mu \cdot e(m) \cdot u(m), \tag{17}$$

where μ is the adaptation parameter which determines the speed and stability of adaptation. To control j ARM amplitudes, j sets of independent adaptive controllers are needed, as illustrated in Fig. 3.

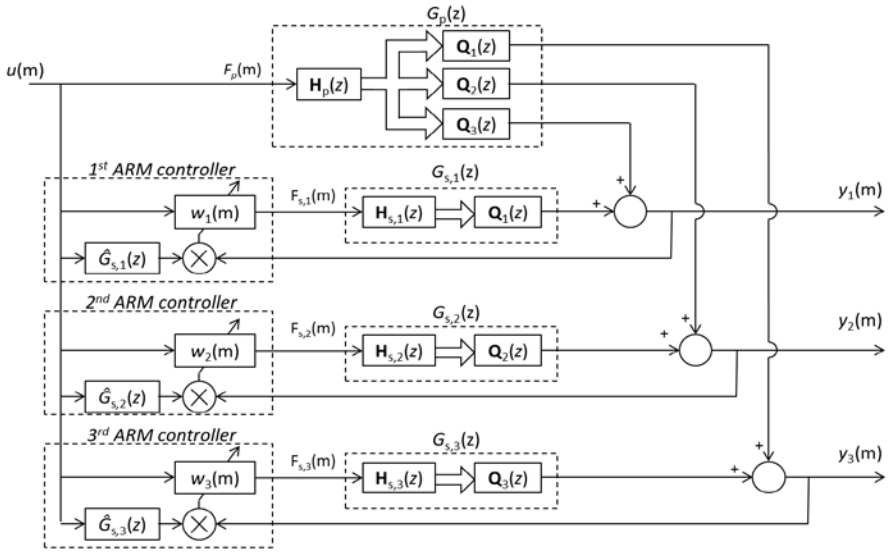

Figure 3: Block diagram representation of the adaptive feedforward ASAC using FxLMS algorithm

5. Numerical simulations

Real-time simulations were performed using Matlab® and Simulink®. A baffled rectangular steel plate of size 400 mm x 300 mm x 2 mm, clamped at all edges, is used as a reference model. Other simulation parameters are given in Table 1. For these parameters, there are 12 vibration modes and 8 acoustic radiation modes with efficiency more than 0.1 in the frequency range $0.1f_n$ to $0.9f_n$.

Table 1: Parameters used in the simulations

Parameter	Value	Parameter	Value
Sampling frequency f_s	2 kHz	Poisson's ratio ν	0.3
Nyquist frequency $f_n = f_s/2$	1 kHz	Density of air, ρ_0	1.239 kg m^{-3}
Loss factor η	0.01	Speed of sound in air, c_0	340 m s^{-1}
Density of plate ρ	7800 kg m^{-3}	Order of the controller filter	40
Young Modulus of plate E	200 GPa	Order of the estimator filter	40

5.1 Estimation of acoustic radiation modes and radiated sound power

The causal delayed version of the non-causal filters discussed in Section 3 are constructed in time domain using 23rd order FIR filters with 11-samples delay. These FIR filters are designed by a least-squares fit to the ideal frequency responses at 1000 uniformly spaced frequency bins up to the Nyquist frequency, i.e. 1000 Hz, with uniform weighting. The performance of these filters in estimating the ARMs at the location (120.0 mm, 182.5 mm) on the plate can be seen in Fig. 4(a)-(b). It is clearly shown that causal delayed versions of the non-causal FIR filters estimate the magnitudes of the ARMs better while the phase is linearly approximated, which represents the time delay. It must be noted for adaptive control, introduction of small filter delays is not important as it will just add delay in the adaptation which can be included in the FxLMS scheme.

Figure 4(c) shows the radiated sound power when the structure is excited by a random primary point force, F_p (band-passed filtered using a 5th order elliptical filter with normalised edge frequencies of 0.1 and 0.9 of Nyquist frequency) acting at (45 mm, 60 mm). Twenty sensors uniformly distributed on the plate are used to measure the real-time surface velocities. The sensor transfer functions are represented in time domain using a set of modal filters, each designed by 3rd order IIR filters.

The estimates of the ARM amplitudes are found by filtering the time series of the sensor outputs with the causal delayed versions of the non-causal ARM filters, before summing them. The radiated sound power is then estimated by multiplying the squares of the estimates of the ARM amplitudes

with the corresponding eigenvalues. A detailed explanation of radiated sound power estimation can be found in Section 4 of [6]. The comparison of the radiated sound power given in Fig. 4(c) is made between the theoretical approach from Eq. (1) and the approach based on the time domain estimation of ARMs discussed in Section 3. It can be seen that the radiated sound power is estimated well across the whole frequency band of interest.

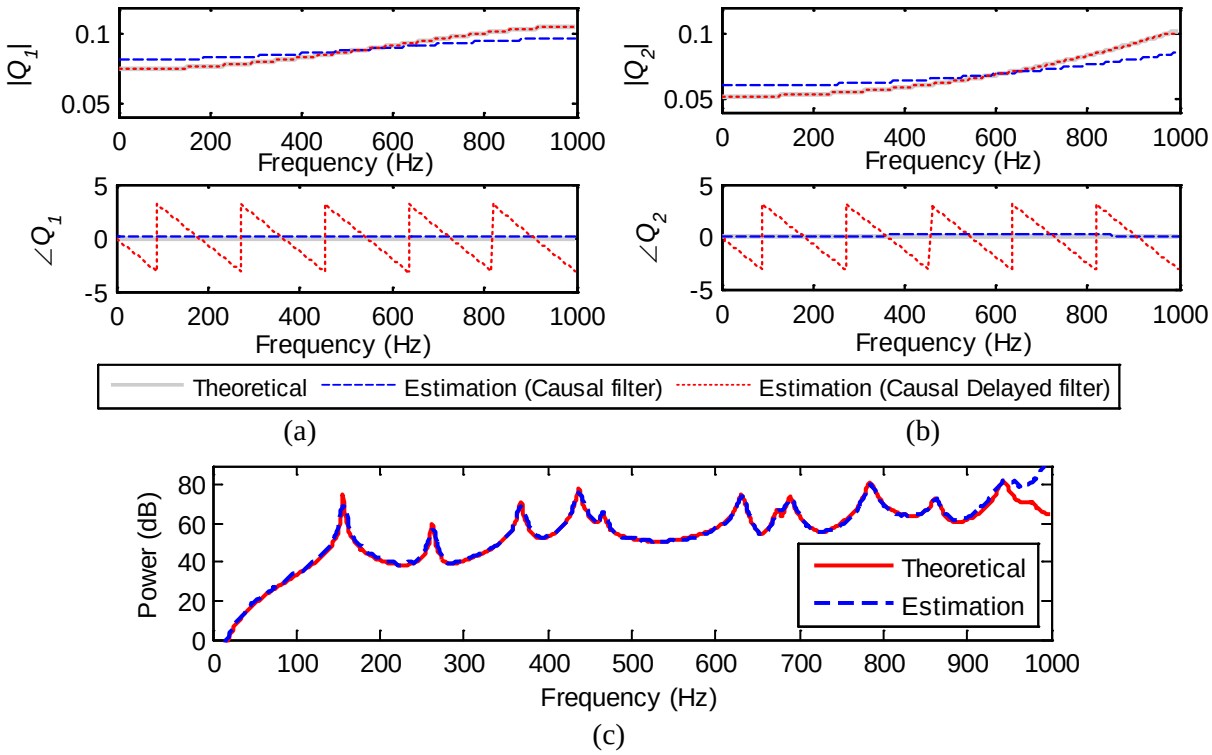

Figure 4: Estimation of (a) the 1st ARM, (b) 2nd ARM and (c) radiated sound power

5.2 Performance of adaptive controllers

Simulations of the adaptive control were run for 500s, with the average responses over a 100s period from t = 400s being found. The locations of the three secondary forces, $F_{s,1}$, $F_{s,2}$ and $F_{s,3}$ are (200 mm, 150 mm), (340 mm, 45 mm) and (60 mm, 255 mm), respectively. Here, three cases are considered, i.e. (i) cancellation of the first ARM (ii) cancellation of the first 2 ARMs, and (iii) cancellation of the first 3 ARMs. Step-sizes for the adaptation were set as $\mu_{1,2,3} = 0.0001$.

Figure 5 shows the results of applying these three control cases. The average reductions of the radiated sound power achieved from case (i), (ii) and (iii) within the frequency range $0.1f_n$ to $0.5f_n$ are 6.5 dB, 9.0 dB and 9.9 dB, respectively. The reductions of the radiated sound power at the natural frequencies of the plate are presented in Table 2. It can be seen that substantial attenuation is achieved at the first natural frequency due to the high radiation efficiency of the first ARM. Moreover, cancellation of more ARMs increases the attenuation and widens the control bandwidth.

Table 2: Reduction of the radiated sound power at the natural frequencies of the plate

Natural frequencies (Hz)		156	262	368	437	466	631	675	689
Attenuation (dB)	Case (i)	32.3	1.6	-0.1	21.9	0.3	0.1	-0.3	2.7
	Case (ii)	29.4	3.3	20.8	15.4	2.0	15.0	1.6	5.1
	Case (iii)	32.2	5.5	22.1	14.3	1.7	15.8	0.5	5.3

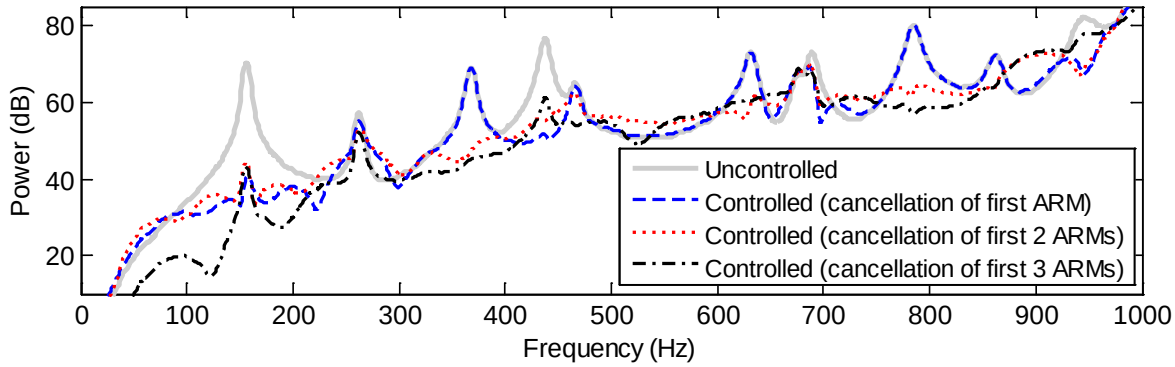

Figure 5: Adaptive control of radiated sound power

6. Concluding Remarks

This paper is an extension of the work presented in [6], whereby the focus is on developing FxLMS controllers to adaptively control the sound power radiated from a vibrating, rectangular clamped plate. The ARM estimation approach was applied to this two-dimensional radiator and performed very well in estimating the frequency-dependent ARMs and the radiated sound power.

The proposed FxLMS controllers were able to reduce the 3 targeted ARM amplitudes, hence reducing the overall radiated sound power over a frequency range including 12 modes of vibration. The proposed control strategy achieves 32 dB attenuation at the first natural frequency of the plate and 9.9 dB on average.

It is important to highlight that the performance of the proposed approach might differ in practical applications due to computation time associated with long filter taps/delays and the large number of sensors involved. These and other issues are reported elsewhere.

REFERENCES

1 Elliott, S. J. and Johnson, M. E. Radiation modes and the active control of sound power, *The Journal of the Acoustical Society of America*, **94** (4), 2194-2204, (1993).

2 Cunefare, K. A. The minimum multimodal radiation efficiency of baffled finite beams, *The Journal of the Acoustical Society of America*, **90** (5), 2521-2529, (1991).

3 Berkhoff, A. P. Broadband radiation modes: Estimation and active control, *The Journal of the Acoustical Society of America*, **111** (3), 1295-1305, (2002).

4 Maillard, J., *Advanced time domain sensing for active structural acoustic control*, Virginia Polytechnic Institute and State University, (1997).

5 Wu, W. Analysis of acoustic radiation mode in time domain, *Science in China Series E: Technological Sciences*, **52** (8), 2384-2390, (2009).

6 Nor, K. A. M., Mace, B. and Hioka, Y. Time-domain estimation of acoustic radiation modes and active structural acoustic control, *Acoustics 2016: The Second Australasian Acoustical Societies' Conference*, (2016).

7 Mao, Q. and Pietrzko, S. *Control of Noise and Structural Vibration: A MATLAB®-Based Approach*, Springer Science & Business Media, (2013).

8 Sung, C.-C. and Jan, C. T. Active control of structurally radiated sound from plates, *The Journal of the Acoustical Society of America*, **102** (1), 370-381, (1997).

9 Mace, B. R. and Halkyard, C. R. Time domain estimation of response and intensity in beams using wave decomposition and reconstruction, *Journal of Sound and Vibration*, **230** (3), 561-589, (2000).

10 Elliott, S. J. 2 - Optimal and Adaptive Digital Filters. *Signal Processing for Active Control*. Academic Press, London, (2001).